Princeton Plasma Physics Laboratory

PPPL- 4911

PPPL- 4911

# SPIRAL Field Mapping on NSTX for Comparison to Divertor RF Heat Deposition

Joel Hosea, et. al.

June, 2013

PPPL PRINCETON PLASMA PHYSICS LABORATORY

Prepared for the U.S. Department of Energy under Contract DE-AC02-09CH11466.

# Princeton Plasma Physics Laboratory
# Report Disclaimers

---

## Full Legal Disclaimer



## Trademark Disclaimer



---

# PPPL Report Availability

## Princeton Plasma Physics Laboratory:

http://www.pppl.gov/techreports.cfm

## Office of Scientific and Technical Information (OSTI):

http://www.osti.gov/bridge

---

**Related Links:**

**U.S. Department of Energy**

**Office of Scientific and Technical Information**

**Fusion Links**

# SPIRAL field mapping on NSTX for comparison to divertor RF heat deposition

J. C. Hosea[a], R. Perkins[a], M. A. Jaworski[a], G. J. Kramer[a], J.-W. Ahn[b], N. Bertelli[a]
S. Gerhardt[a], T. K. Gray[b], B. P. LeBlanc[a], R. Maingi[a], C. K. Phillips[a],
L. Roquemore[a], P. M. Ryan[b], S. Sabbagh[c], G. Taylor[a], K. Tritz[d], J. R. Wilson[a] and the NSTX Team

[a]*Princeton Plasma Physics Laboratory, Princeton University, Princeton, NJ 08543, USA*
[b]*Oak Ridge National Laboratory, Oak Ridge, TN 37831, USA*
[c]*Columbia University, New York, NY 10027, USA*
[d]*Johns Hopkins University, Baltimore, MD 21218, USA*

**Abstract.** Field-aligned losses of HHFW power in the SOL of NSTX have been studied with IR cameras and probes, but the interpretation of the data depends somewhat on the magnetic equilibrium reconstruction. Both EFIT02 and LRDFIT04 magnetic equilibria have been used with the SPIRAL code to provide field mappings in the scrape off layer (SOL) on NSTX from the midplane SOL in front of the HHFW antenna to the divertor regions, where the heat deposition spirals are measured. The field-line mapping spiral produced at the divertor plate with LRDFIT04 matches the HHFW-produced heat deposition best, in general. An independent method for comparing the field-line strike patterns on the outer divertor for the two equilibria is provided by measuring Langmuir probe characteristics in the vicinity of the outer vessel strike radius (OVSR) and observing the effect on floating potential, saturation current, and zero-probe-voltage current ($I_{V=0}$) with the crossing of the OVSR over the probe. Interestingly, these comparisons also reveal that LRDFIT04 gives the more accurate location of the predicted OVSR, and confirm that the RF power flow in the SOL is essentially along the magnetic field lines. Also, the probe characteristics and $I_{V=0}$ data indicate that current flows under the OVSR in the divertor tiles in most cases studied.

**Keywords:** RF heating, Spherical tokamak.
**PACS:** 52.50.Qt, 52.55.Fa.

## INTRODUCTION

The SPIRAL code [1] has been used to provide magnetic field mappings in the scrape off layer (SOL) on NSTX from the midplane SOL in front of the HHFW antenna to the divertor regions, resulting in magnetic field strike point patterns on the divertor which closely match the RF heat deposition spirals measured there [2,3]. These results indicate that the RF power losses to the divertor via the SOL are well aligned with the magnetic field lines passing in front of the HHFW antenna. An important question with regard to RF modeling and understanding the underlying mechanism(s) for this RF power loss channel is exactly how well aligned to the field lines is the loss. SPIRAL mappings for two different magnetic equilibria, EFIT02 [4] and LRDFIT04 [5], have been used to see which equilibrium provides the best matching spiral to the heat deposition spiral for RF plus NBI H-mode plasmas [3]. In this case the spirals for the two equilibria both match the heat deposition spiral rather well to within about 1 cm, with LRDFIT04 giving a better match for R in the divertor $R_{div}$ near the outer vessel strike radius (OVSR) (i.e., for field strike points produced by lines passing nearer the last closed flux surface LCFS in front of the antenna), and with EFIT02 giving a better match farther outboard (i.e., toward field line strike points produced by lines closer to the antenna).

In this paper, SPIRAL field mappings for the two equilibria are compared to the heating spirals produced during an RF only H-mode plasma at elevated power but at modest density to avoid large SOL power deposition [6]. This is followed by an independent comparison of the times predicted for the two equilibria for the OVSR to cross over a set of 4 probes with times at which the effects of the OVSR are observed on the probes [7]. In this latter case, the plasmas are again RF-only-heated, relatively modest density plasmas, and the OVSR is programmed to move out in $R_{div}$ at a speed dependent on the amplitude of $P_{RF}$.

# SPIRAL COMPARISONS TO IR RF HEAT DEPOSITION

The RF-only heated discharge #135253 of Ref. 6 is chosen for the SPIRAL comparisons to IR camera measured RF heat deposition spirals here. Figure 1 shows a visible camera picture of the RF heat deposition spirals on the upper and lower divertor regions for this discharge at t = 0.366 sec, and presents the corresponding SPIRAL field line strike maps evaluated with the LRDFIT04 equilibrium at t = 0.361 sec. The conditions are HHFW H-mode, $P_{RF}$ ~ 3.7 MW, $B_T$ = 0.55 T, $I_P$ = 0.65 MA, helium, $k_{||}$ = -8m$^{-1}$, $\phi_{Ant}$ = -90°, and for t = 0.365 s, $T_e(0)$ = 5.8 keV, $n_e(0)$ ~ 1.6 $10^{19}$ m$^{-3}$, and $n_e$(R = 1.562 m, 1.3 cm in front of the antenna) ~ 0.6 $10^{18}$ m$^{-3}$. This edge density is close to the cutoff density of 0.5 $10^{18}$ m$^{-3}$ for which condition the efficiency of the RF heating of the core plasma is relatively high [8,9] and the RF peaks from the hot spiral zone are expected to be small relative to the lower divertor heat deposition caused by exhaust from the core plasma. The comparisons of the SPIRAL maps for LRDFIT and EFIT to IR heat deposition taken for IR cameras at Bay I (slow, 30 Hz frame rate) and Bay H (fast, 3.774 kHz frame rate) are shown in Fig. 2. The background heat deposition is caused by the exhaust from the core plasma and the RF heat deposition spiral produces the small peaks noted in the figure. The OVSR for LRDFIT is ~ 4.5 cm inboard of that for EFIT in this case. The inner RF peak is clearly resolved, especially for the fast IR data in Fig. 2b, just outboard of the LRDFIT OVSR as in Ref. 3, and definitively shows that the LRDFIT OVSR is the correct value since the EFIT OVSR falls in the vessel gap. This data again shows that LRDFIT gives the best match at $R_{div}$ approaching the OVSR.

Comparison results are shown in Fig. 3 for the upper divertor IR RF heat measurements δQ at Bay G. Here the LRDFIT spiral matches the RF heat deposition best at both the $R_{div}$ near the OVSR and at the outer radii corresponding to field lines passing within a few centimeters of the antenna surface. At the relatively low magnetic

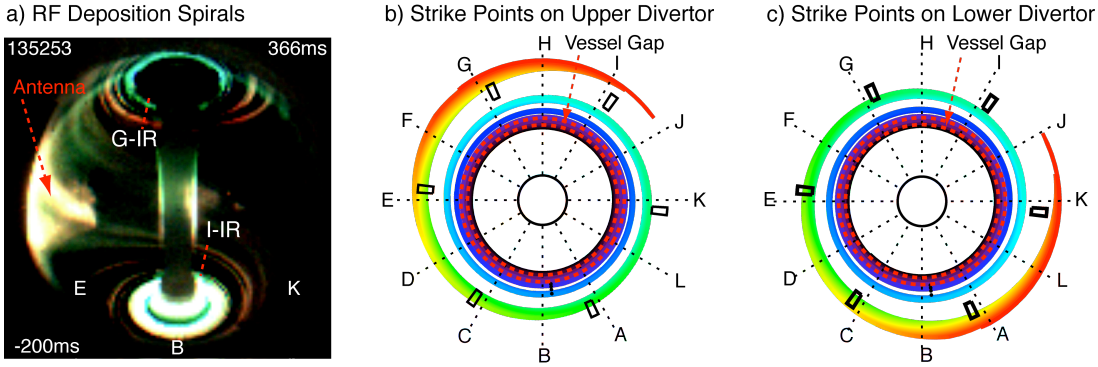


Fig.1 (a) RF power deposition spirals on the divertors are closely matched by SPIRAL mappings of strike points on the (b) upper and (c) lower divertors for field lines passing in front of the antenna in the SOL. [Scale of dashed radii in (b) and (c) is ~ 1 m.]

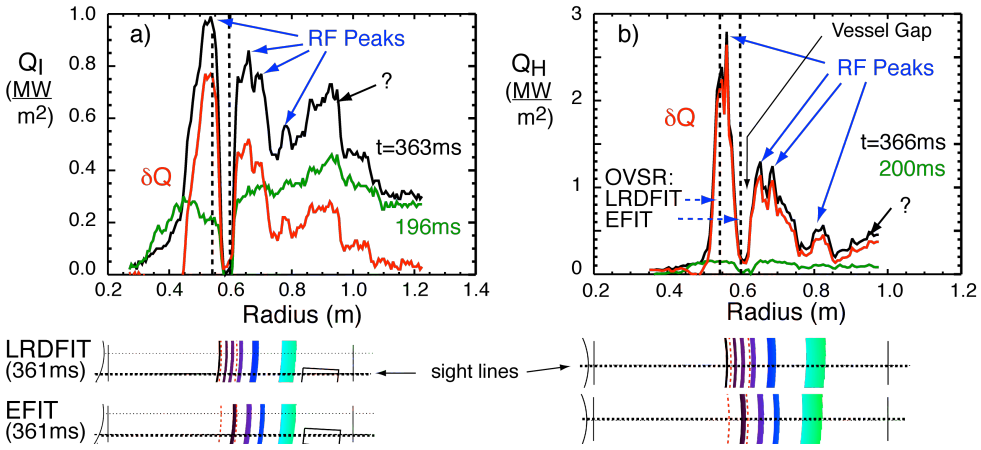


Fig. 2. LRDFIT04 and EFIT02 spiral strike point mappings compared with lower divertor IR heat flux measurements with a) the slow IR camera at Bay I for t = 0.363 sec, and b) the fast IR camera at Bay H for t = 0.366 sec. The OVSR for LRDFIT is inboard of that for EFIT by ~ 4.5 cm as is indicated by the vertical dashed lines. (Shot # 135253)

pitch for this discharge, the SPIRAL field line strike map is rotated so that the outer part of the spiral falls at Bay G [3] (also see Fig. 1).

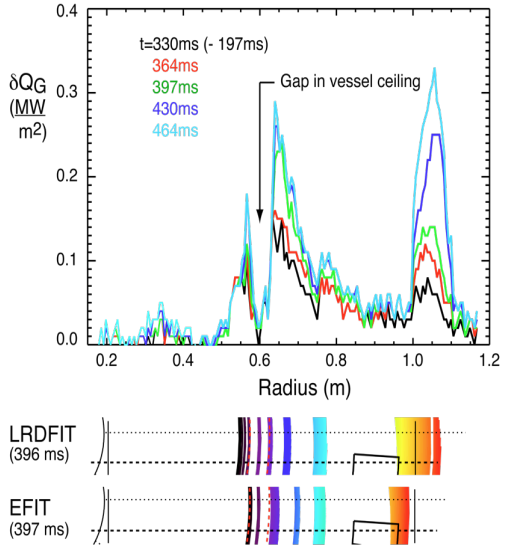


Fig. 3. LRDFIT04 (0.396 s) and EFIT02 (0.397s) spiral strike point mappings compared with upper divertor IR incremental heat flux measurements parallel to R at several times. Shot # 135253.

## LOCATION OF OVSR WITH PROBES

Four Langmuir probes are located just outboard of the lower vessel gap at Bay B at R = (1) 0.638 m, (2) 0.647 m, (3) 0.675 m and (4) 0.706 m, and the plasma OVSR is swept over these probes [7] at a rate depending on the RF power level. Figure 4 shows versus time (a) the probe currents $I_{V=0}$ ($|V_P| < 0.5$ V), (b) the probe floating potentials $V_f$ ($|I_P| < 1$ mA), and (c) the locations of the OVSR predicted by EFIT and by LRDFIT for two separate evaluations, LRDFIT_1 and LRDFIT_2. Vertical dashed lines indicate presumed OVSR crossings where $I_{V=0}$ and $V_f$ are approximately zero. LRDFIT clearly matches these crossings best and LRDFIT_1 indicates a dithering which coincides with the second ramp in both $I_{V=0}$ and $V_f$ for probe 3. The correspondence of the zero crossing of these parameters to the OVSR is clearer in Fig. 5. $I_{V=0}$, $V_f$, and $I_{sat}$ ($V_{P1} < -47.5$ V) for probe 1 are shown for several RF power levels. [Conditions for Fig. 5 are the same as Fig. 4 but with $n_{e1.562m}(10^{18}m^{-3})$: $n_{e1.00m}(10^{19}\ m^{-3})$: $T_{e1.00m}$(keV) = (a) 0.3: 2.1: 2.5, (b) 0.5: 2.7: 1.3, (c) 1.2: 2.9: 0.57.] $I_{V=0}$ and $V_f$ both cross 0 at the cross over of the OVSR. Importantly, LRDFIT predicts the crossover times very well whereas EFIT predicts the crossover time well for $P_{RF} = 0$ but deviates markedly as $P_{RF}$ is increased. At the crossover times, the predicted OVSR values minus the probe 1 radius (ΔR) for LRDFIT and EFIT are shown in Table 1. The ΔR values for LRDFIT are considerably smaller than those for EFIT, which in turn appear to increase with RF power.

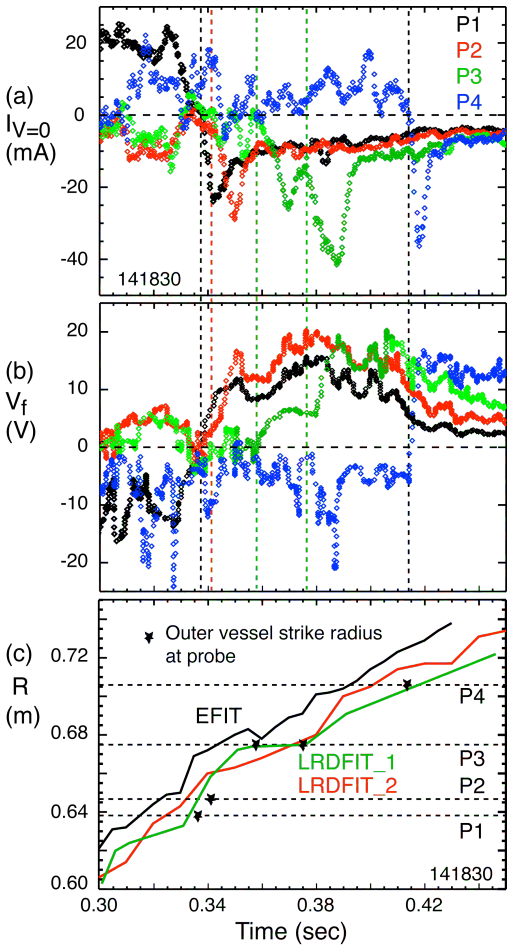


Fig. 4. Four probe array measurements of (a) $I_{V=0}$ and (b) $V_f$ vs time during the sweep of the OVSR across them as indicated by c) OVSR R from EFIT and LRDFIT equilibria. Conditions similar to those of Section II except $P_{RF}$ = 0.53 MW and $n_e(0) \sim 2.7\ 10^{19}\ m^{-3}$.

Also, the changing of sign of $I_{V=0}$ at the OVSR in Fig. 5 indicates that current flows under the OVSR. This current is in addition to the current that can flow around the periphery of the plasma [10] and through the vessel [11] between the outer and inner strike regions. The IV characteristics for Fig. 5a for times before and after the OVSR crossover are shown in Fig. 6. These clearly show the current reversal about the OVSR. The exponential fits to the characteristics are: $I_{sat}$(mA), $V_f$(V), $T_e$(eV) = 50, -30, 50 for $R > R_{OVSR}$ and = 55, 23, 14 for $R < R_{OVSR}$.

**TABLE (1)**: Deviation of the OVSR predicted from the probe 1 radius for LRDFIT and EFIT at the crossovers in Fig. 5

| Fig 5 | $P_{RF}$(MW) | ΔR(cm) LRDFIT04 | ΔR(cm) EFIT02 |
|---|---|---|---|
| (a) | 1.1 | 0.4 | 4.1 |
| (b) | 0.53 | 0.9 – 1.7 | 3.2 |
| (c) | 0 | - 0.6 | 1.2 |

The characteristics in Fig. 6 have been smoothed against high frequency turbulence fluctuations using the IDL "smooth" operator with w = 5. The probe current perturbations which remain during the one millisecond sweep times for the characteristics are similar to those observed on edge soft x-ray signals [6]. This suggests that these probe current perturbations are possibly due to plasma fluctuations at the divertor plate.

## CONCLUSION

The comparisons between SPIRAL mappings and IR RF heat deposition spirals, as well as between OVSR location predictions and crossing effects on probes, clearly support the conclusion that the LRDFIT equilibrium gives the best matches in both cases. The very good match between the OVSR crossover time predicted by LRDFIT and the OVSR crossover time measured for probe 1 versus power in Fig. 5 is an independent check on the equilibrium that is then used to provide SPIRAL maps which match the IR RF heat deposition very closely. This result reinforces our conclusion that the RF power flow in the SOL from in front of the antenna to the divertor regions flows along the magnetic field lines. This is an important conclusion for testing advanced RF codes that include the SOL open magnetic field line region.

## ACKNOWLEDGEMENTS

The authors wish to acknowledge the support of Dr. Masayuki Ono and Dr. Jonathan Menard, the NSTX team and the machine, RF, and neutral beam operations groups. This work is supported by USDOE Contract No. DE-AC02-09CH11466.

## REFERENCES

1. G. Kramer *et al., Plasma Phys. Contr. F.* **55**, 0250136 (2013).
2. R.J. Perkins *et al., PRL* **109**, 045001 (2012).
3. R.J.Perkins *et al., Fusion Energy Conf.,* EX/P5-40 (IAEA 2012).
4. S. Sabbagh *et al., Nucl. Fusion* **41**, 1601 (2001).
5. J. Menard, PPPL, private communication.
6. J.C. Hosea *et al., 38th EPS Conf. on Plasma Physics,* P2.098 (2011).
7. J. Kallman *et al., RSI* **81**, 10E117 (2010).
8. J.C. Hosea *et al.*, *Physics of Plasmas* **15**, 056104 (2008).
9. J.C Hosea *et al*., *AIP Conf. Proceedings* **1187**, 105 (2009).
10. A. Kumagai *et al.,* PPCF **39**, 1189 (1997).
11. A. Kallenbach *et al.,* J. Nuclear Materials **290-293**, 639 (2001).

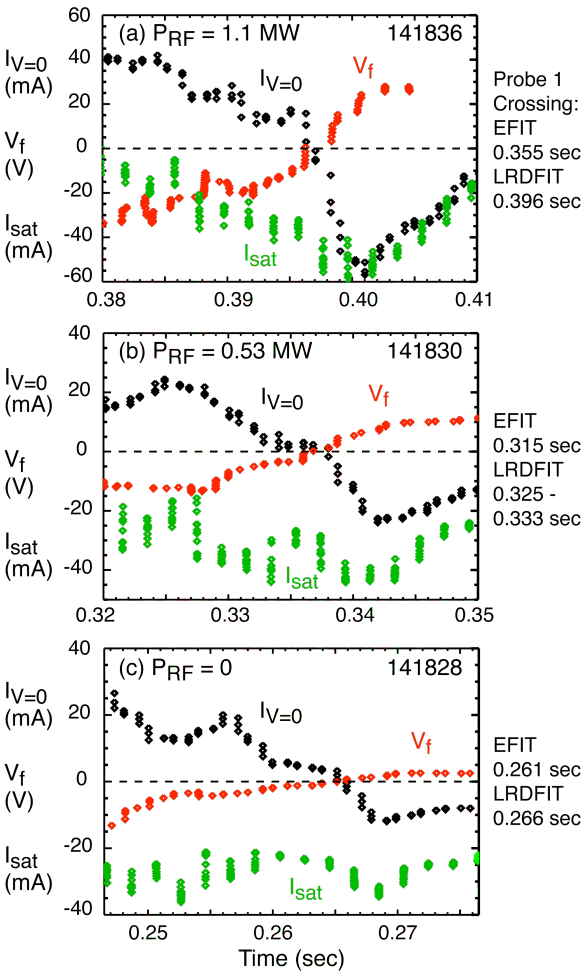


Fig. 5. Probe 1 crossover characteristics, $I_{V=0}$, $V_f$, and $I_{sat}$, versus time for (a) $P_{RF}$ = 1.1 MW, (b) $P_{RF}$ = 0.53 MW, and (c) $P_{RF}$ = 0.

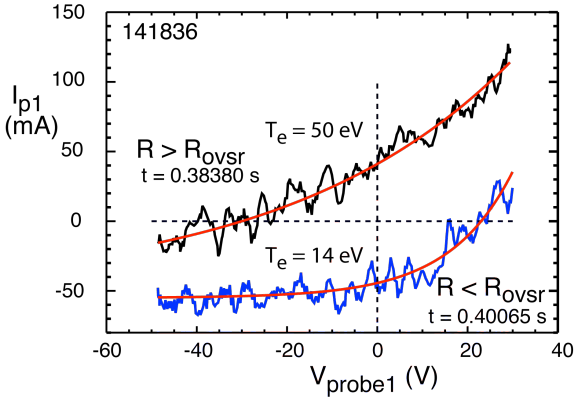


Fig. 6. Probe 1 characteristics for R > the outer vessel strike radius $R_{ovsr}$, and for R < $R_{ovsr}$. The electrons are cooler and the current at $V_{probe1}$ = 0 clearly changes direction in the private flux region. (IDL "smooth" operator with w = 5 is used here.)

The Princeton Plasma Physics Laboratory is operated
by Princeton University under contract
with the U.S. Department of Energy.

Information Services
Princeton Plasma Physics Laboratory
P.O. Box 451
Princeton, NJ 08543

Phone: 609-243-2245
Fax: 609-243-2751
e-mail: pppl_info@pppl.gov
Internet Address: http://www.pppl.gov